

Time scaling in the convection onset of a supercritical fluid

H. MEYER ^a and G. ACCARY ^b

a. Department of Physics, Duke University, Durham, NC 27708-0305, USA

b. Holly Spirit University of Kaslik, Jounieh, Lebanon

Résumé :

L'article présente une revue des expériences et des simulations numériques du développement de la convection de Rayleigh-Bénard dans une couche de fluide supercritique, ^3He , après l'application en $t=0$ d'un flux de chaleur constant q sur la paroi inférieure. Les expériences ont été réalisées le long de l'isochore critique pour différentes proximités du point critique et plusieurs valeurs de q , et la différence de température $\Delta T(t)$ dans la couche de fluide a été mesurée. Les résultats montrent que les différents temps caractéristiques t_i observés sur le profil de $\Delta T(t)$ ainsi que le temps caractéristique du développement de la convection déterminé numériquement, exprimés à travers t_i/τ_D , peuvent être représentés en fonction du nombre de Rayleigh, où τ_D est le temps caractéristique de diffusion thermique. Une démonstration réalisée par Michael Cross (non publiée) montre d'une manière générale la possibilité d'une telle représentation et sera discutée ici. Une comparaison des profils de $\Delta T(t)$ obtenus expérimentalement et numériquement est présentée également et des différences non élucidées encore sont discutées.

Abstract:

A review is presented on the laboratory experiments and simulations on the convection onset of a supercritical fluid, ^3He , in a Rayleigh-Bénard cell after the start of a steady heat flow q from the bottom wall at the time $t=0$. The experiments were conducted at several temperatures along the critical isochore and over a wide range of q , and measured the temperature drop $\Delta T(t)$ across the fluid layer. It was empirically found that the various characteristic times t_i observed in the profile of $\Delta T(t)$, and also in the convection growth determined by numerical simulations, could each be expressed by t_i/τ_D as function of the Rayleigh number, where τ_D is the diffusive relaxation time. This scaled representation is to be expected, as has been shown in a general demonstration by Michael Cross (unpublished) and its implications are discussed. A comparison of the profiles $\Delta T(t)$ from experiments and simulations are presented and various unresolved discrepancies will be discussed.

Keywords: Supercritical fluid, Rayleigh-Bénard convection, Numerical simulation

1 Introduction and presentation of results

The dynamics of equilibration and the convection in supercritical fluids is of great interest because of their diverging compressibility as the critical point is approached, and many laboratory experiments, predictions and simulations on the equilibration of these fluids have been carried out especially over the past twenty years (see for instance [1,2]). Over the last ten years, studies of supercritical ^3He have focused on the transient from equilibrium to fully developed convection [3,4,5], and in this report a review is given on the results. An assessment is presented of the problems and discrepancies that remain to be solved.

The experiments were carried out with a Rayleigh-Bénard cell, and the fluid space of the circular cell had a diameter of 57 mm and a height of 1 mm, hence the aspect ratio was $\Gamma = 57$. The cell was made of pure, very high conductivity copper, with flat polished surfaces for the upper and lower plates, and thin stainless steel walls. In the simulations the cell height was also taken as $L = 1$ mm, with values of Γ between 4 and 20, and periodic vertical boundaries were used. A steady heat flow q was started from the bottom wall at time $t=0$. In the experiments, the temperature drop $\Delta T(t)$ across the fluid layer was measured, to be compared with the results from simulations. The critical point temperature of ^3He is $T_c = 3.318$ K, and experiments and simulations were carried out along the critical isochore for values of the reduced temperature $\varepsilon = (T_i - T_c)/T_c$ from 0.01 to 0.2, where T_i is the initial temperature. Over this range, the compressibility decreases by a

factor of about 38, and the Prandtl number from 38 to 2.1. The experimental result analysis and the simulations used the published data of the ^3He static and dynamic properties.

As expected, the profile of $\Delta T(t)$ was found to be a strong function of q and of ε , but the most striking feature, observed both in the experiment and in the simulations, are the damped oscillations after the initial sharp rise of $\Delta T(t)$. In Fig.1-a a representative plot of $\Delta T(t)$ obtained experimentally is shown with the definition of characteristic times, and in Fig. 1-b, a comparison is made between simulation and experiment under the same conditions of ε and q .

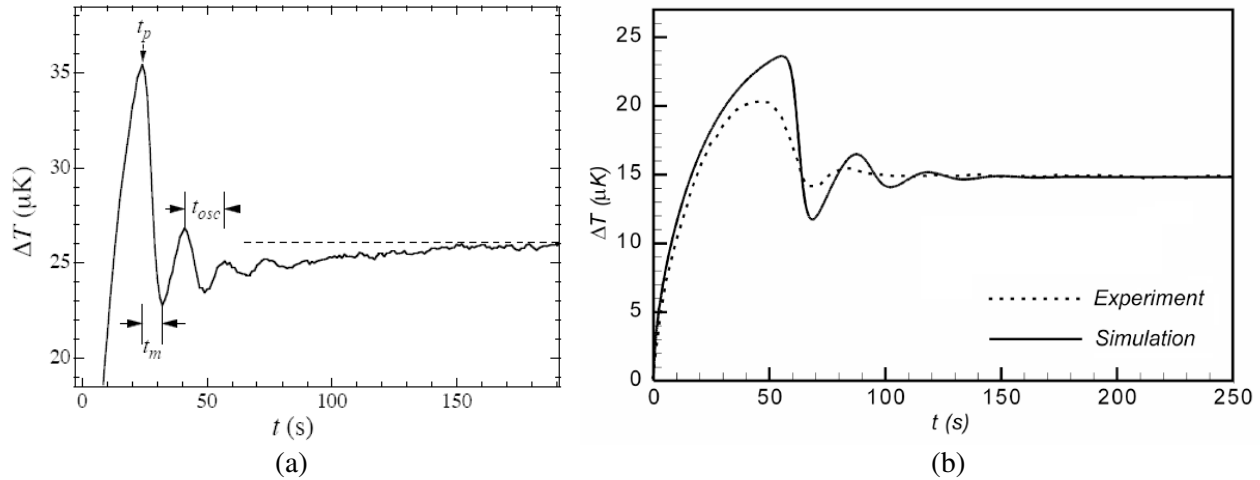


FIG. 1 – (a) A representative profile $\Delta T(t)$ after starting the heat current with the definition of the times t_p , t_{osc} , and the slow exponential relaxation to the steady-state value of ΔT (dashed line) with a time constant τ_{tail} for $\varepsilon = 0.02$ with the heat flow $q = 1.69 \times 10^{-7} \text{ W/cm}^2$ and where $\Delta T(t=0) = 0$ (from [6]). (b) A comparison of $\Delta T(t)$ between simulation and experiment for $\varepsilon = 0.05$ and for $q = 4.58 \times 10^{-8} \text{ W/cm}^2$ with a small temperature perturbation applied on the top wall in the simulation to match the value of t_p (from [7]).

In the experimental data plot, the features defining “characteristic times” t_i are shown. These are (i) the period t_{osc} of the oscillations, (ii) the time t_p of the first peak, and (iii) the asymptotic relaxation time to the steady-state convection, τ_{tail} .

- i) The oscillations result from the high compressibility of the fluid, which leads to the enhanced “piston effect”, a thermo-acoustic effect, and they are progressively damped and disappear as the compressibility diminishes when ε is increased. Amiroudine and Zappoli [8] have presented a detailed description and discussion on the oscillations in the profile of $\Delta T(t)$ as caused by the piston effect. The convective “warm” fluid motion upwards to the “cold” boundary leads to a thermo-acoustic effect which drives fluid downwards leading to the first peak in the $\Delta T(t)$ profile at the time t_p . The cooler mass propagating downwards towards the warm lower horizontal boundary leads again to a “piston effect” effect, driving “warm” fluid upwards, and producing a minimum in $\Delta T(t)$, and so on.
- ii) The maximum at the time t_p indicates that convection has developed substantially, and t_p is much larger than the convection onset time t_{ons} where the fluid has been predicted to become unstable [9]. Its value is not only a function of the fluid static and transport properties (at the distance ε to the critical point) and the cell dimensions, but also depends on other factors such as non-ideality of the flat cell, static perturbations such as sharp corners at the cell boundaries. The larger these perturbations are, the smaller the ratio t_p/t_{ons} . In the absence of such perturbations, the fluid would in principle remain in an unstable state, without convection setting in.
- iii) The asymptotic relaxation tail with the characteristic time τ_{tail} always tends from below towards the steady-state convection value ΔT_{ss} (for t large enough). This is opposite to the direction observed for weakly compressible fluids (an example is given in Fig. 10-a) of [10].
- iv) In addition, simulations give information on the convection intensity growth through the calculation of the mean enstrophy in the fluid volume, with a growth rate $\sigma = (1/t_{conv})$, as shown in Fig. 2 for a representative example. Here the enstrophy En_s is defined as:

$$Ens = \sum_{i,j=1}^3 \frac{1}{2} (v_{i,j} - v_{j,i})^2 \quad (1)$$

where v_{ij} represents the derivative of the velocity component v_i in the direction j and is a measure of the rotational strength of fluid motion.

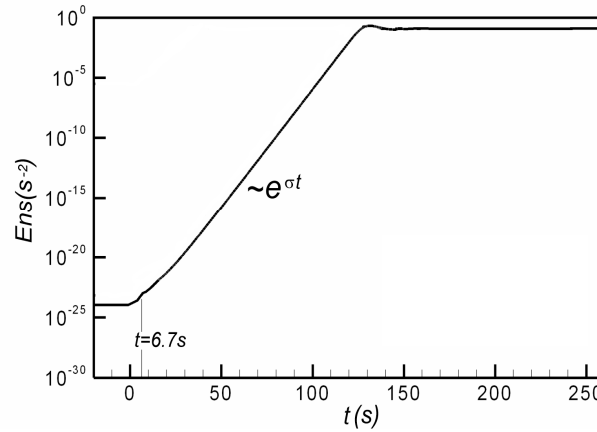


FIG. 2 – Time evolution of the space-averaged enstrophy for $\varepsilon = 0.2$ and $q = 0.216 \text{ mW/cm}^2$. After the fluid layer has become unstable (at $t = 6.7 \text{ s}$), the mean enstrophy increases exponentially with time with a rate σ (from [4]).

The general observation of the four times t_i just described is that for a given initial temperature on the critical isochore, they all decrease with increasing heat flow (or equivalently with increasing ΔT_{ss}) and this will be discussed further below. A qualitative argument to explain this behaviour is that with increasing q the critical Rayleigh number is reached more rapidly after starting the heat flow at $t = 0$, leading to a faster beginning to fluid instability. This in turn causes a faster development of convection, accelerating the action from piston effect causing the oscillations and driving the fluid faster toward steady-state convection.

For direct comparison with experiments, numerical simulations are based on the same fluid property values as in the experiment and the same value of L . They use the hydrodynamic equations derived and used by Furukawa and Onuki (Eqs 2.8 and 2.17 in [5]) or by Accary (Eqs VI-1 to VI-4 in [7]). Comparing the plots of $\Delta T(t)$ obtained from experiment and from simulations in different research groups shows that the convection develops more slowly than in the experiment. In the simulations, the perturbations causing the convection to develop beyond the instability point depend on the noise in the simulation program. The effective perturbation by this noise is smaller than that in the experimental cell, and hence in simulations t_p is larger than in experiments. This is particularly evident at smaller values of Ra . However by imposing a very small temperature perturbation on one of the horizontal boundary plates in the simulation programming, the development of the convection is accelerated. A single value selected for the perturbation amplitude will then get t_p to be consistent with the experimentally observed one (Fig. 1-b) in all the plots of $\Delta T(t)$ [4,6].

As can be seen in Fig. 2, the enstrophy growth can be represented by a straight line on a semi-log plot of the mean enstrophy versus time, permitting the definition of the growth rate σ . The enstrophy tends to a constant value when steady-state convection has been reached. The location in time where the slope of the curve sharply changes and becomes horizontal is close to t_p .

It was found empirically that the data for each of these characteristic times t_i could be expressed by a scaled representation:

$$t_i / \tau_D = F_i(Ra_{corr} - Ra_c) \quad (2)$$

where $\tau_D = L^2/4D$ is the diffusive relaxation time, D is the thermal diffusivity, Ra_{corr} is the Rayleigh number corrected for the effect of compressibility (as presented for instance in [3],[5] and [6]) and $Ra_c = 1708$ is the critical Rayleigh number. As shown in Fig. 3 the scaling functions F_i are quite different for each of the characteristic times. However a common behaviour is that they all decrease with increasing Ra_{corr} . It should be noted from these figures that in the experiments and simulations, the values of Ra_{corr} extended up to about 5×10^6 , hence into the domain of early turbulence.

We note in passing that in the steady-state convection the $\Delta T_{ss}(q, \varepsilon)$ results could also be expressed [6] by a scaling relation $j_{corr} = \Phi (Ra_{corr} - Ra_c)$, where j_{corr} is the dimensionless convection current defined in [11], and corrected as described in [6]. This is the ratio of the convective portion of the heat current to that conducted through the fluid at the transition, where the data are compared with predictions from simulations, and good agreement was obtained.

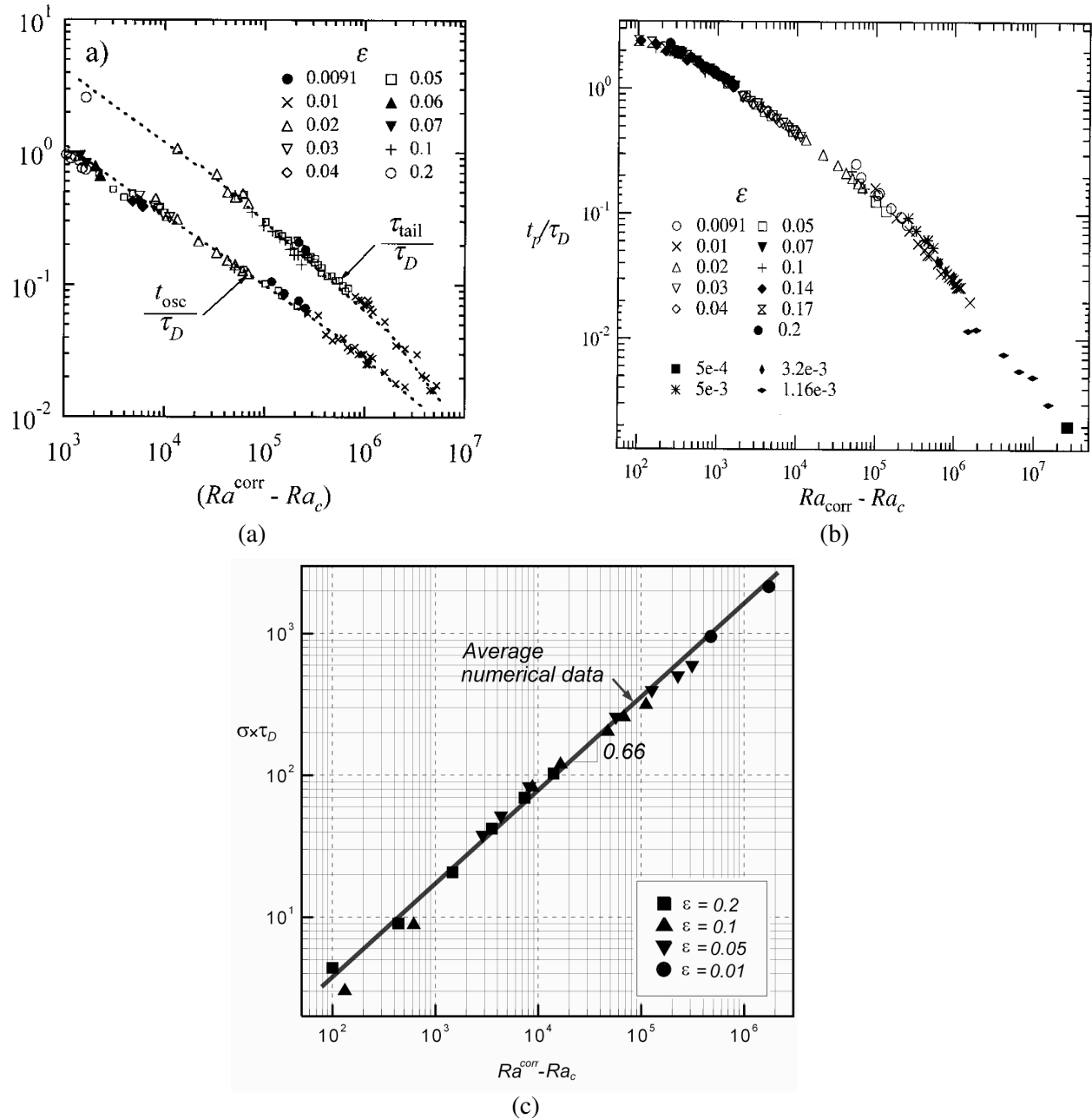


FIG. 3 – Representation of the scaled times t_{osc} , t_p , τ_{tail} and σ versus $(Ra_{corr} - Ra_c)$ (from [4] and [6]).

2 Discussion of the results

2.1 Scaling of characteristic times

A demonstration by Michael Cross [12] provides a general justification of the empirical scaling expression Eq. (2). It assumes that the various thermodynamic derivatives and kinetic coefficients are constant during the heat flow at constant top plate temperature. This condition is realized to a good approximation in the experiments, because the values of Ra used were sufficiently low. M. Cross started from the hydrodynamic

equations (2.8 and 2.17) of [5], and introduced dimensionless variables. He used the boundary conditions at the top and bottom plates of the Rayleigh-Bénard cell and then found that the only parameters of the so-transformed equations are the dimensionless numbers Ra_{corr} , Pr , α_s , and Γ , where $\alpha_s = 1 - C_v/C_p$, the ratio of the specific heats at constant volume and pressure. The hydrodynamic equations then lead to the prediction that for any time scale t_i , one obtains a general expression of the form:

$$t_i / \tau_D = F_i(Ra_{corr}, Pr, \alpha_s, \Gamma) \quad (3)$$

The experiment analysis however is only able to detect the dependence on Ra_{corr} . That on Pr is too weak to be observed, although Pr varies by a large amount over the experimental range. It might be possible that for our range of Prandtl numbers, the dependence on Pr is smaller than it might be for lower values of Pr [12]. Because only one cell with a single value of Γ was used, the dependence on Γ could not be tested. As for α_s , it varies from 0.85 for $\varepsilon = 0.2$ up to 0.99 for $\varepsilon = 0.01$, and its impact on the scaling could not be determined.

2.2 Comparison of the observed and simulated profiles $\Delta T(t)$

There is in general qualitative agreement, as can be seen from a sample shown in Fig.1-b, and in particular there is good agreement between the steady-state value of ΔT (ΔT_{ss}) and the recorded and simulated oscillatory times t_{osc} . However there are notable discrepancies, some mentioned earlier:

- a) The location t_p of the first peak in $\Delta T(t)$ is dependent on the perturbations that lead to the development of convection. These are different in the simulations and in the experiments, and hence the t_p in the experiments is smaller than in the simulations, as already mentioned earlier. This effect is particularly large for small values of Ra , but diminishes with increasing Ra . By introducing an additional perturbation of the same amplitude into all the simulations [4,6], all the values of t_p from experiment and simulations can be made to agree. However this generic perturbation does not explain the real physical situation of the perturbation in the experimental cell.
- b) The slow relaxation of $\Delta T(t)$ to the steady-state convection value with time τ_{tail} is not observed in simulations, where the decay of the oscillations is less rapid than in the experiments, and their amplitudes appear to be symmetric about the final steady-state value ΔT_{ss} .
- c) For low values of Ra over a certain range of ε , no full oscillations are observed, only what appear to be “truncated” oscillations. As seen from the dotted line in Fig.4a, the steady-state value of ΔT is reached once its negative slope has changed discontinuously to zero after the first peak at t_p . By contrast, simulations always show full oscillations. This might be an instrumental effect from the cell boundary wall in the experiments, as suggested by M. Cross [12]: After the heat flow is switched on, the convection rolls are believed to start from the circular cell boundary and propagate with a constant front speed towards the centre. This gradual progression – axi-symmetric or not, if the cell is not perfect – might cause a monotonous change of the bottom plate temperature with time. Here the Nusselt number might increase roughly linearly with time, until the steady-state convection is reached throughout the cell. Thus full oscillations of $\Delta T(t)$ are suppressed. This explanation [12] would be valid for incompressible fluids, but it is not known what the impact of the piston effect would be. In the 2D simulations, by contrast, there are no perturbing effects from the “periodic boundaries”, the motion of the convection rolls are all in phase and not influenced by cell imperfections, and hence the oscillations are not truncated.
- d) The damping of the oscillations is larger in the experiments than in the simulations. This again might be an instrumental effect due to the not-perfect geometry of the cell.

2.3 Further problems to be understood

In this short review only the results over the critical-point proximity range $9 \times 10^{-3} < \varepsilon < 0.2$ have been discussed. At smaller values of ε , several observations were made [3], with unexpected results, and which need further study:

- a) The damped oscillations with characteristic times t_{osc} were no longer observed, and also the profile $\Delta T(t)$ was found to be different from that for $\varepsilon > 9 \times 10^{-3}$.

- b) For these high Prandtl numbers ($Pr > 40$), the Nu (Ra_{corr}) profile for $Ra_{corr} > 10^7$ was found to be anomalous. Unfortunately, the experiments had to be terminated before these unexpected observations could be repeated and studied further. It is our hope that these intriguing problems will be addressed in the future.

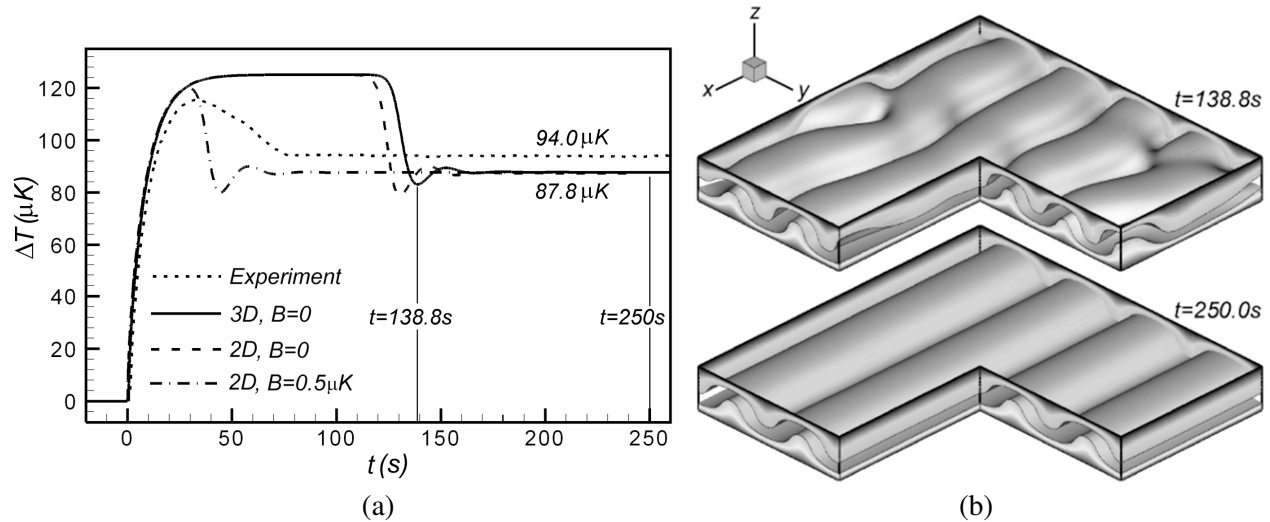


FIG. 4 – (a) Time evolution of the temperature difference $\Delta T(t)$ for $\varepsilon = 0.2$ and $q = 0.216 \mu W/cm^2$, from experiment (dotted line) and simulations without ($B=0$) and with perturbation of the temperature of the top plate (B is the amplitude of perturbation). The heating starts at $t = 0$ (from [4]). (b) Cuts of the temperature fields corresponding to the 3D simulation shown in (a) carried out for an aspect ratio of 8 with periodic lateral boundaries, the temperature field at $t = 250$ s corresponds to steady-state, the lower and upper shaded isotherms correspond to $T-T_i = 10 \mu K$ and $5 \mu K$ respectively.

Acknowledgments

The authors are much indebted to Michael Cross for his demonstration of scaling, (Eq. 3), and for additional illuminating and insightful correspondence.

References

- [1] B. Zappoli. Near-critical fluids hydrodynamic. C. R. Méc., 331, p. 731, 2003.
- [2] H. Meyer, F. Zhong. Equilibration and other dynamic properties of fluids near the liquid-vapor critical point. C.R. Méc., 332, p. 327, 2004.
- [3] A.B. Kogan, H. Meyer. Heat transfer and convection onset in a compressible fluid: 3He near the critical point. Phys. Rev. E, 63, 056310, 2001.
- [4] G. Accary and H. Meyer. Perturbation-controlled numerical simulations of the convection onset in a supercritical fluid layer. Phys. Rev. E, 74, 046308, 2006.
- [5] A. Furukawa and A. Onuki. Convective heat transport in compressible fluids. Phys. Rev. E, 66, 016302, 2002.
- [6] A. Furukawa, H. Meyer, A. Onuki, A.B. Kogan. Convection in a very compressible fluid: Comparison of simulations with experiments. Phys. Rev. E, 68, 056309, 2003.
- [7] G. Accary. Convection de Rayleigh-Bénard dans les fluides supercritiques : Mécanismes d'instabilité et transition vers la turbulence. PhD thesis, Université de la Méditerranée d'Aix-Marseille II, 2005.
- [8] S. Amiroudine, B. Zappoli. Piston-effect-induced thermal oscillations at the Rayleigh-Bénard threshold in supercritical 3He . Phys. Rev. Lett., 90, 105303, 2003.
- [9] L. El Khouri, P. Carlès. Scenarios for the onset of convection close to the critical point. Phys. Rev. E, 66, 066309, 2002.
- [10] R.P. Behringer. Rayleigh-Bénard convection and turbulence in liquid-helium. Rev. Mod. Phys. 57, p. 657, 1985.
- [11] G. Ahlers, M. Cross, P. Hohenberg and S. Safran. The Amplitude Equation Near the Convection Threshold: Application to Time-Dependent Heating Experiments. J. Fluid Mech. 110, p. 297, 1981.
- [12] M. Cross, unpublished notes and private communications (2008).